Advanced InSAR atmospheric correction: MERIS/MODIS combination and stacked water vapour models

Zhenhong Li*†, Eric J. Fielding‡, Paul Cross♣, and René Preusker§

†: Department of Geographical and Earth Sciences, University of Glasgow, UK

‡: Jet Propulsion Laboratory, California Institute of Technology, Pasadena, California, USA

♣: Department of Civil, Environmental and Geomatic Engineering, University College London, UK

§: Institut für Weltraumwissenschaften, Freie Universität Berlin, Germany

Abstract. A major source of error for repeat-pass Interferometric Synthetic Aperture Radar (InSAR) is the phase delay in radio signal propagation through the atmosphere (especially the part due to tropospheric water vapour). Based on experience with the GPS/MODIS integrated [*Li et al.*, 2005] and the MERIS correction models [*Li et al.*, 2006c], two new advanced InSAR water vapour correction models have been demonstrated using both MERIS and MODIS data: (1) The MERIS/MODIS combination correction model (MMCC); and (2) the MERIS/MODIS stacked correction model (MMSC). The applications of both the MMCC and the MMSC models to ENVISAT ASAR data over the Southern California Integrated GPS Network (SCIGN) region showed a significant reduction in water vapour effects on ASAR interferograms, with the RMS differences between GPS and InSAR derived range changes in the LOS direction decreasing from ~10 mm before correction to ~5 mm after correction, which is similar to the GPS/MODIS integrated and the MERIS correction models. It is expected that these two advanced water vapour correction models can expand the application of MERIS and MODIS data for InSAR atmospheric correction. A simple but effective approach has been developed to destripe Terra MODIS images contaminated by radiometric calibration errors. Another two limiting factors on the MMCC and MMSC models have also been investigated in this paper: (1) the impact of the time difference

between MODIS and SAR data; and (2) the frequency of cloud free conditions at the global scale.

1. Introduction

Atmospheric water vapour effects represent one of the major limitations of repeat-pass interferometric SAR (InSAR), especially for small amplitude geophysical signals with long wavelengths including interseismic deformation and some anthropogenic processes. *Zebker et al.* [1997] suggested that a 20% spatial or temporal change in relative humidity could result in a 10-14 cm error in deformation measurement retrievals, independent of baseline parameters.

Space-based monitoring is an effective way to obtain a measurement of water vapour distribution on a global basis with a high spatial resolution, and calibration techniques to spatially reduce path delays using either the NASA Moderate Resolution Imaging Spectroradiometer (MODIS) or the ESA MEdium Resolution Imaging Spectrometer (MERIS) data have been successfully demonstrated [*Li et al.*, 2005; 2006c].

MODIS is a passive whisk broom scanning imaging spectroradiometer on the Terra and Aqua satellites, launched on 18 December 1999 and 4 May 2002, respectively. MODIS provides global coverage every 1-2 days with observations in 36 spectral bands at moderate resolution (0.25 - 1 km). Five near IR MODIS channels are used for remote sensing of water vapour with a 1-km spatial resolution over clear land areas, oceanic areas with Sun glint, and/or above clouds over both land and ocean [*Gao and Kaufman*, 2003]. It is shown that MODIS appeared to overestimate water vapour against GPS with a scale factor of 1.05, indicating that MODIS water vapour should be calibrated (e.g., using a linear model) before being applied to correct InSAR water vapour effects [*Li et al.*, 2003]. After calibrating using a GPS-derived linear fit model, it is found that MODIS and GPS water vapour products agreed to within 1.6 mm in terms of standard

deviations [*Li*, 2004]. *Li et al.* [2005] reported that, after calibrating their scale uncertainty using GPS data, two or more MODIS near IR water vapour fields can be adopted to produce Zenith Path Delay Difference Maps (ZPDDM) for InSAR atmospheric correction, and this was designated as the GPS/MODIS integrated water vapour correction model.

Launched together with the Advanced Synthetic Aperture Radar (ASAR) on the ESA ENVISAT spacecraft on 1 March 2002, MERIS is a passive push-broom imaging instrument and measures the solar radiation reflected from the Earth's surface and clouds in the visible and near IR spectral range during the daytime [*ESA*, 2004]. MERIS has two out of fifteen narrow spectral channels in the near IR for the remote sensing of water vapour either above land or ocean surfaces under cloud free conditions [*Bennartz and Fischer*, 2001] or above the highest cloud level under cloudy conditions [*Albert et al.*, 2001]. MERIS near IR water vapour products are available at two nominal spatial resolutions: 0.3 km for full resolution (FR) mode, and 1.2 km for reduced resolution (RR) mode. Spatio-temporal comparisons show c. 1.1 mm agreement between MERIS and GPS/radiosonde water vapour products in terms of standard deviations [*Li et al.*, 2006d]. In *Li et al.* [2006c], MERIS-only near IR data was used to reduce water vapour effects on ASAR interferograms.

Application of both the GPS/MODIS integrated and the MERIS correction models to ERS/ASAR data over the Los Angeles region showed that the order of water vapour effects on interferograms can be reduced from ~10 mm to ~5 mm after correction. The MERIS near IR water vapour product has several advantages for correcting ASAR measurements over MODIS data for ERS-2 or ASAR data: 1) A time difference usually exists between MODIS and SAR data, whereas MERIS data is acquired at the same time as ASAR data; 2) MERIS full-resolution mode has better spatial resolution, up to

0.3 km against 1 km for MODIS; 3) MERIS and ASAR have a virtually identical propagation path, whilst MODIS does not.

On the other hand, MERIS cannot detect clouds as well as MODIS so the MODIS cloud mask is more robust, particularly when the clouds are thin. This is because measurements over 14 channels with wavelengths between 0.659 μm and 13.935 μm are used in the MODIS cloud mask algorithm to estimate whether a pixel is cloudy or not [*Ackerman et al.*, 1998], whilst MERIS is limited to wavelengths between 0.4 μm and 0.9 μm, and very valuable thermal information and information on liquid and ice water absorption at 1.6μm and 3μm are not available. Imperfections in the MERIS cloud mask particularly in mountainous areas, were highlighted by a recent study [*Li et al.*, 2006c]. Moreover, MODIS Level 2 processed data usually only has a latency period of ~1 day with free public access and FTP orders are usually filled within 24 to 48 hours. In contrast, ESA keeps a copyright on its data, and it can take more than 2 weeks to receive MERIS data products on physical media.

Therefore, it is clear that MODIS and MERIS near IR water vapour products are complementary for correcting interferograms and it is expected that the combination of MODIS and MERIS near IR water vapour products can expand the application of MERIS and MODIS data for InSAR atmospheric correction. In this paper, based on experience with the GPS/MODIS integrated [*Li et al.*, 2005] and the MERIS correction models [*Li et al.*, 2006c], we evaluate two advanced MERIS/MODIS correction models as well as the impact of the time difference between MODIS and SAR data on MODIS-based/related correction models. In this paper, the term "MODIS-based correction models" refers to water vapour correction models using GPS-calibrated MODIS data only (i.e. the GPS/MODIS integrated model demonstrated in *Li et al.* [2005]) whilst "MODIS-related models" refers to water vapour correction models using both MODIS

and MERIS data (i.e. the two advanced correction models to be discussed in this paper; which can also be referred to as "MERIS-related models"). Similarly, "MERIS-based correction models" refers to water vapour correction models using MERIS data only, i.e. the correction model demonstrated in *Li et al.* [2006c].

2. Two advanced MERIS/MODIS water vapour correction models

Based on data availability and data quality, two water vapour correction models, using both MERIS and MODIS data, can be employed to produce Zenith Path Delay Difference Maps (ZPDDM) for InSAR atmospheric correction.

When MERIS data collected on date 1 and MODIS data collected on date 2 are available, or vice versa, ZPDDM can be derived as follows:

(1) In order to remove the scale uncertainty, MODIS Precipitable Water Vapour (PWV) values derived from near IR measurements require calibration using a linear correction model that can be derived from data collected at one or more continuous GPS (CGPS) stations [*Li et al.*, 2003, 2005].

(2) MERIS and MODIS PWV values need to be converted into zenith wet delays (ZWD) using surface temperature measurements that can be obtained from one or more meteorological stations including radiosondes and/or GPS [*Li*, 2005];

(3) Both MERIS and MODIS ZWD fields should be resampled to a common uniform geographic grid of c. 300 m;

(4) A ZPDDM is calculated by differencing MERIS and MODIS 2D ZWD fields; It should be noted that the dry delay (i.e. the phase delay due to dry air) is either assumed to be unchanged or offset only by a constant between SAR data acquisitions;

(5) Since MERIS and MODIS near IR water vapour products are sensitive to the presence of clouds, there are often missing values in the resultant ZPDDM, which can be filled in using the cloud-free ZWD differences with an improved inverse distance weighted interpolation method (IIDW) [*Li*, 2004];

(6) In order to suppress the inherent noise of MERIS and MODIS PWV measurements (the band ratios used in their water vapour retrieval algorithms tend to enhance noise), a low-pass filter can be applied to the ZPDDM such as a boxcar averaging window with a width of ~2.0 km. Assuming pixel to pixel water vapour errors are uncorrelated, the accuracy of the ZPDDM increases by a factor of 2 at the expense of spatial resolution. Since the agreement between MERIS/MODIS and GPS is within ~1.6 mm [*Li*, 2005; *Li et al.*, 2003, 2006d], assuming both water vapour products have the same accuracy as GPS, and taking into account the conversion factor (around 6.2) to convert PWV to ZWD, and the factor of 2 due to the use of the low-pass filter, it can be concluded that the uncertainty in the resultant ZPDDM is around 5 mm ($(1.6/\sqrt{2}) \times 6.2 \times \frac{1}{2} \times \sqrt{2} = 5$ mm). Assuming an incidence angle of 23 degrees, the uncertainty in the ZPDDM could lead to an error of ~5 mm in deformation estimates in the line of sight direction.

In this paper, we designate this first MERIS/MODIS combination correction model as MMCC. The MMCC model can be adopted when either MERIS or MODIS data is not available for a date, or when their cloud masks perform poorly. There are two possible combinations for the MMCC model: (1) MERIS data from date 1 and MODIS data from date 2; and (2) MODIS data from date 1 and MERIS data from date 2.

A second approach is similar to InSAR phase stacking [*Zebker et al.*, 1997; *Fialko*, 2004; *Wright et al.*, 2004]. When both MERIS and MODIS data are available for one or

both dates and the impact of the time difference between them can be considered negligible, simple averaging of both water vapour fields is expected to reduce the noise. If the noise level in two water vapour fields is the same, averaging of these independent images can statistically reduce the noise of the original individual water vapour fields by a factor of $\sqrt{2}$, and this is designated as the MERIS/MODIS stacked correction (MMSC for short) model hereafter in this paper. When producing a ZPDDM, the only difference between the MMSC and the MMCC models involves the introduction of an additional step to average MERIS and MODIS ZWD fields before Step (3) in the MMSC model. When both water vapour fields are available on both dates, the MMSC-derived ZPDDM should statistically have less noise (by a factor of $\sqrt{2}$) than the MMCC-derived one. When both water vapour data sources are only available for one of the days, the MMSC-derived ZPDDM will still have less noise (this time by a factor of $\sqrt{3}/2$) than the MMCC-derived one. There are five possible combinations for the MMSC model: (1) [MERIS + MODIS] (date 1) + [MERIS + MODIS] (date 2); (2) [MERIS + MODIS] (date 1) + MERIS (date 2); (3) [MERIS + MODIS] (date 1) + MODIS (date 2); (4) MERIS (date 1) + [MERIS + MODIS] (date 2); and (5) MODIS (date 1) + [MERIS + MODIS] (date 2).

3. Applications of the MMCC and MMSC models over the SCIGN region

Three pairs of ESA ENVISAT ASAR images over the Los Angeles region on the descending (satellite moving south) track 170 were processed from the ASAR level 0 (raw data) products using the ROI_PAC (version 2.3) software [*Rosen et al.*, 2004], and precise satellite orbits from Delft University (Netherlands) [*Scharoo and Visser*, 1998]. Effects of topography were removed from the interferograms using a 1-arc-second (~30 m) posting digital elevation model (DEM) produced by the Space Shuttle Radar Topography Mission (SRTM) [*Farr and Kobrick*, 2000].

Figure 1 shows the flowchart of InSAR processing with the MMCC correction model. In order to reduce water vapour effects on the interferograms, a ZPDDM derived in Section 2 should be inserted into the interferometric processing sequence after removing the topographic phase contribution. The ZPDDM is mapped from the geographic coordinate system to the radar coordinate system (range and azimuth) and subtracted from the interferogram. This corrected interferogram can be unwrapped and then an adjusted baseline can be estimated by minimizing the difference between the unwrapped phase and a simulated phase map from the DEM [*Rosen et al.*, 2004]. In order to obtain the unwrapped water-vapor-corrected interferogram, a new simulated interferogram is created using the refined baseline and topography, and is subtracted from the unwrapped phase (including orbital ramp) with the water vapour model removed.

In order to properly reduce water vapour effects on interferograms, the step of mapping ZPDDM from the geographic coordinate system to the radar coordinate system (range and azimuth) (see Figure 1) is crucial [*Li et al.*, 2006b]. Using information from a precise DEM and the satellite orbit, a radar image (in the SAR range-azimuth coordinates) can be simulated so that its amplitude depends on the local topographic slope and the SAR geometry. As part of this SAR image simulation, a mapping table is generated mapping each geographic location to the corresponding range-azimuth coordinates. Then the parameters of an affine transformation between the simulated and actual SAR images can be calculated by fitting offsets determined by using a cross-correlation matching algorithm to adjust for any unmodelled geometric parameters [*Massonnet and Feigl*, 1998; *Rosen et al.*, 2000]. With the simulation mapping table and affine transformation parameters, the ZPDDM can be mapped from the geographic coordinate system to the SAR coordinate system (range and azimuth). A recent validation study using 10 corner reflectors over Rosamond Dry Lake in California

showed that a matching accuracy of ~1 SAR pixel (i.e. ~20 m) can be obtained [*Li, et al.*, 2006a], which is consistent with [*Massonnet and Feigl*, 1998] (about half the size of a DEM pixel, i.e. ~15 m). Bearing in mind that the spatial resolution of the ZPDDM is ~2 km, the uncertainty due to matching errors can be neglected.

In topographic mapping, a first-order or second-order approximation is commonly used for the relationship between the elevation of the terrain and the observed phase with the Earth reference considered locally flat [*Lin et al.*, 1991; *Zebker and Goldstein*, 1986]. *Abdelfattah and Nicolas* [2002] stated that this approximation could introduce an error of 1.66 m in the path difference even for a small area (50 km by 50 km) and the third order should not be ignored for high-precision DEM generation. Because a single SAR image can cover a wide region (e.g. 100 km by 100 km for a standard ERS/ENVISAT image), the impact of Earth curvature has to be taken into account. In the JPL/Caltech ROI_PAC software that we use, earth curvature is handled for deformation mapping by subtracting a synthetic phase calculated for a surface of constant elevation or using a surface digital elevation model based on a given ellipsoid reference, projected into the SAR image coordinates at the same time as the simulated amplitude image described above [*Rosen et al.*, 2000]. The phase calculation includes the effect of Earth curvature on the projection of the baseline between the two orbits, and the change of baseline along-track. The excellent agreement between the ZPDDM and the interferogram also implies that the approximation impact is negligible for InSAR water vapour correction models.

It has been demonstrated in several previous studies [e.g. *Bawden et al.*, 2001; *Watson et al.,* 2002; *Lanari et al.*, 2004; *Argus et al.,* 2005] that the Los Angeles region surface deformation exhibits seasonal oscillations, anthropogenic motions, and tectonic

movements, and that the most rapid movements are non-tectonic deformations due to groundwater and petroleum fluid level changes. *Argus et al.* [2005] reported that the southeast part of the Santa Ana aquifer exhibited seasonal vertical movements of up to 136 mm with horizontal seasonal motions of up to 8 mm during the period from 1998 to 1999. In order to validate the MMCC and MMSC models, independent 3D GPS-derived displacements provided by the Scripps Orbit and Permanent Array Center (SOPAC) [*Nikolaidis,* 2002] were compared with InSAR results in the satellite line of sight (LOS) direction for a pixel at the same location as the GPS station over the SCIGN region. Note that the a posteriori root-mean-square (RMS) noise of the SOPAC precise GPS station coordinates is claimed to be nearly 1 mm (horizontally) and 3.5 mm (vertically) [*Nikolaidis*, 2002] and hence the uncertainty in the station coordinates in the ground-to-satellite line of sight is c. 3.2 mm (assuming an incidence angle of 23 degrees). It is believed that: (1) temporal filtering used in GPS data processing makes it preferred to derive range changes in the line of sight from the station coordinates, i.e. the uncertainty in range changes is less than $3.2 \times \sqrt{2} = 4.5$ mm; (2) regional filtering used in GPS data processing makes it optimal to compare with InSAR derived range changes. In this paper it should be noted that: (1) the unwrapped phase has been converted to range change in millimetres and positive range change means ground moving away from satellite (if there is no atmospheric effect or any other error); and (2) the unwrapped phase has been shifted by the mean difference between InSAR and GPS range changes when compared to GPS-derived range changes in the LOS direction (as InSAR has no absolute reference datum).

3.1. Interferogram 030927-050129

Figure 2 shows a long-term interferogram spanning 409 days between 27 September 2003 and 29 January 2005 that we call Ifm1. As shown in Table 1, the perpendicular

component of the interferometric baseline of Ifm1 varies from 217 m to 247 m along the track, and the error in the topographic component of the interferometric phase can be up to 1.21 radians (i.e. 0.54 cm in the LOS range changes, assuming 7 metres of DEM error). While the DEM error component could be large and difficult to remove, areas of steep slope and high elevation (where DEM errors are largest) in this interferogram have very low interferometric correlation due to the long baseline [*Fielding et al.*, 2005] and are masked out (gray in the figures), mitigating the DEM errors.

Figure 3(a) shows a MERIS water vapour field collected at 18:00 UTC on 27 September 2003, and Figure 3(b) shows a MODIS water vapour field collected 65 minutes later. Their differences are shown in Figure 3(c) after conversion to Zenith Path Delay Differences. It should be noted that: (1) the ZPDDM in Figure 3(c) illustrates the impact of time difference (65 minutes for this specific case) between MODIS and ASAR data on the water vapour correction models using MODIS data collected on 27 September 2003; (2) the flatter the ZPDDM (i.e., more homogeneous atmosphere), the less the impact of the time difference on the MODIS-based/related correction models; and (3) such a ZPDDM derived from MERIS and MODIS fields collected on the same date is not used for reducing water vapour effects on interferograms, but only for assessing temporal water vapour variations so as to check the impact of time difference. It is clear in Figure 3(c) that the ZPDDM is generally flat except for the southwest flank of the Santa Ana Mountains (SAM) and the yellow and red at the edge of the coastal cloudbank in the southwest of Figure 3(c). The southwestern boundary is most likely due to a failure to identify partially cloudy pixels in the MERIS water vapour field (Figure 3(a)) with the official ESA MERIS cloud mask: (1) The edge in Figure 3(c) is exactly the same as that in Figure 3(a); (2) Thin or broken clouds are much more likely on the edges of cloudy areas than somewhere else; (3) False identification of clouds

results in low values over these pixels due to the fact that the solar radiation backscattered from the top of clouds travels a shorter distance than that backscattered from the Earth's surface, and the low values in Figure 3(a) led to high values in the ZPDDM (i.e. those shown in yellow/red). As shown in Figure 2(a), the coherence over the SAM is very low, thus the spatio-temporal water vapour variation over the southwest flank of the SAM had no (or limited) impact on the water vapour correction models using the specified MODIS water vapour field.

The MERIS and MODIS images for 29 January 2005 were acquired 5 minutes apart (see Figures 3(d) and 3(e)). The comparison between these two images shows little difference over pixels identified as "cloud free" by both MERIS and MODIS cloud mask products (Figure 3(f)). However, the percentage of cloud free pixels identified by MERIS cloud mask is much greater than that by MODIS cloud mask. It appears that cloudy pixels were falsely identified as cloud free in the official ESA MERIS cloud mask (Figure 3(d)). This seems more likely than an error in the MODIS cloud mask of the same scene (Figure 3(e)). The actual cloud status for MODIS and MERIS on this date is expected to be similar for the following reasons: (1) the time difference between these two image acquisitions is only 5 minutes; and (2) the temporal water vapour variation was small during that period (Figure 3(f)).

Figures 2(b) and 2(c) show the corrected interferogram (Ifm1) after applying MERIS-based and MODIS-based water vapour correction models respectively. In Figures 2(b) and 2(c), black solid triangles represent GPS stations where the differences between InSAR and GPS range changes are either *within* or *beyond* a 1-sigma range both before and after correction; white squares with black borders represent GPS stations only when differences are *greater* than 1-sigma before correction, but *within* a 1-sigma range after

correction (i.e. white squares with black borders imply improvement after correction); red solid circles represent GPS stations only when differences are *within* a 1-sigma range before correction, but *greater* than 1-sigma after correction (i.e. red solid circles indicate deterioration after correction). It should be noted that the 1-sigma range was obtained by comparing with GPS derived range changes in the satellite LOS direction in this study. There are 13 white squares and 1 red solid circle after MERIS correction in Figure 2(b), whilst there are 16 white squares and 3 red solid circles after MODIS correction in Figure 2(c), suggesting that both MERIS-based and MODIS-based correction models reduced water vapour effects. It should be noted that all 3 red solid circles in Figure 2(c) are located in mountainous areas with steep slopes where water vapour varies more rapidly and more strongly than across flatter areas, both in space and time. This implies that these 3 red solid circles may be caused by the time differences between MODIS and ASAR data. However, since the water vapour distributions on both dates were stable (Figures 3(c) and 3(f)), the impact of time differences on MODIS-based correction model appear to be generally trivial, particularly over flat areas.

Comparisons between GPS and InSAR range changes in the LOS direction showed that the RMS difference decreased from 0.95 cm before correction to 0.83 cm after the MERIS correction (Figure 2(b)) and to 0.74 cm after the MODIS correction (Figure 2(c)). The MODIS-based correction model appeared to reduce more of the water vapour effects from this interferogram than the MERIS-based correction model, most likely due to the failure to identify thin clouds in the MERIS near IR water vapour product for 29 January 2005 (Figure 3(d)).

Figure 2(d) shows the corrected interferogram after applying the MMSC model. There are 17 white squares and 2 red solid circles in Figure 2(d). Although water vapour signals present in Figures 2(b) and 2(c) can be observed in the corrected interferogram, their amplitude is lessened and there are more white squares (17 against 13 in Figure 2(b) and 16 in Figure 2(c)). The RMS difference between GPS and InSAR range changes in the LOS direction decreased to 0.74 cm after the MMSC correction, which is the same as the result after the MODIS correction. The possible causes are: (1) All uncertainties in MERIS and MODIS water vapour fields were present in the stacked ZPDDM, although the amplitude of the uncertainties became less; and (2) the locations of the GPS stations might result in an underestimation of the performance of the MMSC model.

3.2. Interferogram 040807-050409

Figure 4(a) shows Ifm2 spanning 245 days from 7 August 2004 to 9 April 2005 (Table 1) without water vapour correction, and Figure 4(b) shows the corrected interferogram after applying the MERIS water vapour correction model. Ifm2 has a small perpendicular baseline, and the errors in the SRTM DEM might lead to a phase error of 0.45 radians (i.e. 0.20 cm in the LOS range changes), which can be considered negligible. Note that Ifm2 covers a larger area than Ifm1. From Figures 4(a) and 4(b), it is clear that water vapour effects, particularly north of the San Gabriel Mountains (SGM) and the San Bernardino Mountains (SBM), were significantly reduced after applying the MERIS water vapour correction, with the RMS difference between GPS and InSAR range changes in the LOS direction decreasing from 1.17 cm before correction to 0.60 cm after correction.

Figure 5 shows spatio-temporal water vapour variations on 7 August 2004. There was a strong spatial water vapour variation with a PWV decrease of ~2.5 cm from southeast to

northwest at 18:00 UTC on 7 August 2004 (Figure 5(a)), and it appears that the water vapour moved across San Bernardino Mountains (SBM) and then moved towards the northwest at 18:50 UTC (Figure 5(b)). It is clear in Figure 5(c) that the spatio-temporal water vapour variations during the 50-minute ENVISAT-Terra time difference were significant with path delay differences greater than 5 cm, indicating the MODIS scene was not appropriate to reduce water vapour effects on ASAR measurements on 7 August 2004. In contrast, the water vapour distribution on 9 April 2005 was quite stable, and the path delay differences were similar to each other (not shown). This indicates that the MODIS water vapour field collected on 9 April 2005 is applicable to correct ASAR measurements for water vapour effects, despite a greater time difference of 65 minutes.

In Figure 5(b), some stripes (perpendicular to the Terra MODIS track) can be observed, which are believed to be due to radiometric calibration errors in Terra MODIS sensor array [B.-C. Gao, personal communication, 2005]. MODIS is a cross-track scanning mirror system with blocks of 10 sensors for water vapour channels and the double-sided scan mirror sweeps out a swath of the Earth 10 km wide at nadir in each scan [*Nishihama et al.*, 1997]. Examination of hundreds of Terra MODIS images revealed that stripes consistently appear every ten lines from the second line in MODIS near IR images since 2002 (although their actual impacts on PWV products vary from time to time and from case to case), implying that there are some instrumental errors in Terra MODIS water vapour sensors in the second scanning line. When such a MODIS image is used for atmospheric correction, the impact of stripes is evident on resultant ZPDDMs (e.g. Figure 5(c)) and hence on corrected interferograms (not shown). Therefore, a simple but effective approach is developed to remove the stripes (see Figures 5(e) and 5(f)): (1) since their appearance is regular, it is easy to detect stripes in an orbital

coordinate system (along-track versus across-track); (2) the erroneous values are replaced with interpolated values using the two neighbour pixels in the along-track direction.

In this case study, the MMCC model was used to produce a ZPDDM with MERIS data collected on date 1 (i.e. 7 August 2004) and MODIS data collected on date 2 (i.e. 9 April 2005), and then the ZPDDM was applied to correct ASAR measurements for water vapour effects (Figure 4(c)). After the MMCC correction, the RMS difference between GPS and InSAR range changes in the LOS direction decreased to 0.56 cm (against 1.17 cm without correction), indicating that the MMCC model can reduce water vapour effects on interferograms.

Since both MERIS and MODIS water vapour fields were available and suitable for ASAR atmospheric correction on 9 April 2005, they were averaged to produce a 'stacked' water vapour field, and then combined with the MERIS water vapour collected on 7 August 2004 to generate a ZPDDM for ASAR atmospheric correction (Figure 4(d)). After the stacked water vapour correction, the RMS difference between GPS and InSAR derived range changes decreased to 0.53 cm, which is slightly smaller than the values after the MERIS or the MMCC correction. Moreover, when the MODIS water vapour field collected on 9 April 2005 was used without destriping, stripes can be clearly observed after the MMCC correction whilst they are not present in interferograms corrected with the MMSC model. This suggests that the MMSC model provides the most reliable correction solution for InSAR measurements out of all the correction models discussed here, as expected due to the averaging of the MERIS and MODIS data for date 2 that reduces instrument noise.

3.3. Interferogram 050514-050827

Ifm3 spanning the summer from 14 May 2005 to 27 August 2005 is shown in Figure 6. Like Ifm2 (Figure 4), Ifm3 has a small baseline, and the errors in the SRTM DEM might lead to a phase error of 0.57 radians (i.e. 0.26 cm in the LOS range changes) (Table 1), which can be considered negligible. The RMS of the unwrapped phase decreased from 1.95 rad before correction to 0.79 rad after applying the MERIS-based water vapour correction (Figures 6(a) and 6(b)), indicating that the unwrapped phase was much flatter after correction (below we discuss the remaining signals). Comparison between InSAR and GPS range changes in the LOS showed that the RMS difference decreased from 1.00 cm before correction to 0.41 cm after the MERIS correction.

Both MERIS and MODIS water vapour fields were collected at about 18:00 UTC on 14 May 2005, their time differences were trivial and can be considered negligible. However, the MODIS water vapour field was collected 55 minutes later than MERIS on 27 August 2005, and there was a large temporal water vapour variation during this period. Thus the MMCC model with a combination of (MODIS-MERIS) was applied to correct the ASAR interferogram for water vapour effects. The RMS difference between GPS and InSAR range changes in the LOS direction decreased to 0.51 cm after the MODIS-MERIS correction (Figure 6(c)).

Both MERIS and MODIS water vapour fields collected on 14 May 2005 were averaged to produce a ‘stacked’ water vapour field, and then a ZPDDM was produced using this ‘stacked’ water vapour field with the MERIS water vapour collected on 27 August 2005. The application of the MMSC model to Ifm3 showed that the RMS between GPS and InSAR range changes in the LOS direction decreased to 0.43 cm after correction (Figure 6(d)).

From Figures 6(b), 6(c) and 6(d), it is clear that all three correction models drastically reduced water vapour effects on the original interferogram (Figure 6(a)), and some real geophysical signals were brought out after removing atmospheric water vapour signals:

(1) A range change of ~20 mm in the satellite LOS direction, corresponding to ~22 mm of vertical deformation (assuming no horizontal motion), was observed in Antelope Valley near Lancaster (indicated by a white solid oval) in the summer of 2005, where *Hoffmann and Zebker* [2003] found ~60 mm of land subsidence between January 1996 and January 1999 using both ascending and descending ERS data.

(2) The city of San Bernardino (indicated by a black solid circle) also showed land subsidence of up to 20 mm in the summer of 2005. It should be noted that an uplift of ~10 mm was observed in Ifm2 during the period from 7 August 2004 to 9 April 2005 (Figures 4(b), 4(c) and 4(d)). This indicates that San Bernardino may exhibit seasonal deformation. Note that *Lu and Danskin* [2001] observed seven centimetres of uplift occurred in the same area between December 1992 and August 1993, with four centimetres occurring in only three and a half months during a period of high runoff from surrounding mountains.

(3) An asymmetric 'dumbbell' (corresponding to a surface subsidence of ~20 mm in the satellite LOS direction and indicated by a black dashed oval) was observed in the Long Beach-Santa Ana basin in the summer of 2005. Comparisons between the original interferogram (Figures 6(a)) and the corrected interferograms (Figures 6(b), 6(c) and 6(d)) showed that the right ball of this dumbbell disappeared after correction. However, all previous studies [e.g. *Bawden et al.*, 2001; *Watson et al.*, 2002; *Lanari et al.*, 2004; *Argus et al.*, 2005; *Li et al.*, 2005] showed the summer seasonal subsidence in the Long Beach-Santa Ana basin as an asymmetric dumbbell similar to the shape in Figure 6(a).

In Figures 6(b), 6(c) and 6(d), an additional stripe from the north to the south (indicated by dashed lines) can be observed. This indicates that the stripe caused the asymmetric dumbbell to be erroneously removed. Using pair-wise logic, the conclusion can be drawn that the stripe must come from the MERIS water vapour field collected on 27 August 2005 since it was applied to all three correction models. On closer inspection of the MERIS water vapour fields, it was found that the stripe was present in the 27/08/2005 MERIS water field and its resultant ZPDDMs (Figure 7), providing strong supporting evidence for the conclusion. MERIS comprises 5 identical cameras arranged in a fan-shape configuration in which each camera covers a 14 degree field of view (FOV). A spectral dimension is introduced by imaging the entrance slit of the spectrometer via a dispersing grating onto a Charge-Coupled Device (CCD) array. This leads to small variations of the central wavelength of each band across the field of view of each camera, the so called "smile effect" [*Delwart et al.,* 2007]. Such variation in wavelength can cause disturbances in processing algorithms which, in turn, may lead to visual artefacts ("camera borders", i.e. jumps from one camera to another) [*Delwart et al.,* 2007]. Examination of MERIS water vapour processing revealed that the stripe in Figure 7(b) was due to a camera border between cameras 4 and 5. Note that in-flight spectral calibration campaigns have shown that a spectral slope exists across the FOV for only 4 out of the 5 cameras, whilst camera 4 exhibits very different properties [*Delwart et al.,* 2007]. Since MERIS camera 4 continuously covers one fifth of its whole swath, the effective Terra MODIS destriping approach is not applicable and hence further research to characterise the special behaviour of camera 4 is required. It should be noted that the camera border artefact in the 27/08/2005 MERIS water vapour field is along-track whilst the stripes in MODIS water vapour fields (e.g. Figure 5(b)) are across-track. This is because MERIS is a push-broom imaging spectrometer with 5

Camera Optics Subassemblies (COSA) [*ESA*, 2004] whilst MODIS is a cross-track scanning mirror system with blocks of sensors (10, 20 or 40) for different channels [*Nishihama et al.*, 1997].

4. Global frequency of cloud free conditions

Since both MERIS and MODIS near IR water vapour retrieval algorithms rely on observations of water vapour absorption of near IR solar radiation reflected by land, water surfaces and clouds, they are sensitive to the presence of clouds. Although precipitable water vapour can be retrieved above the highest cloud level under cloudy conditions for both MERIS and MODIS [*Albert et al.*, 2001; *Gao and Kaufman*, 2003], the interests of InSAR applications lie in the full column water vapour values over land rather than clouds. It is therefore useful to assess the frequency of cloud free conditions (i.e. the probability of cloud free occurrence) over land to estimate how often a MERIS/MODIS water vapour correction model might be applicable.

Wylie et al. [1999] investigated the frequency, geographical distribution, and seasonal changes of upper-tropospheric clouds using the High resolution Infrared Radiation Sounder (HIRS) over 8 years (1989-1997) and reported that clear skies were found in 27% of all observations of the Earth from 65°S to 65°N latitude in the boreal summer (June-August) and in only 24% during the boreal winter (December-February). Our recent study shows that the frequency can, for some areas, be much higher than the global average, e.g. 38% for Eastern Tibet [*Li et al.*, 2006d] and 48% for Southern California [*Li et al.*, 2005].

Here, the frequency of cloud free conditions on a global scale is investigated using 6 years of Terra MODIS Atmosphere Monthly Global Product (MOD08_M3). The MODIS Level-3 products (MOD08) contain statistics derived from four Level-2

atmosphere products with different time intervals (daily, eight-day, and monthly): aerosol (MOD04), precipitable water vapour (MOD05), cloud (MOD06), and atmospheric profiles (MOD07). For the daily product, any Level-2 granule that overlaps any part of the data day (0000 to 2400 UTC) is included in the computation of the statistics. The monthly product is computed by manipulating and summarizing the daily product over a calendar month. Statistics are sorted into 1º×1 º cells on an equal-angle global grid (180×360 pixels) [*King et al.*, 2003]. It should be noted that each cell covers an area of ~100 km × 100 km, which is similar to the coverage of a standard ERS SAR or ENVISAT ASAR image in image mode.

Figure 8 shows seasonal frequencies of cloud free conditions on a global scale during the period from March 2000 to February 2006. It is clear that the frequencies varied from place to place and from season to season. The Middle East, North Africa, South Africa, Australia, Chile, Antarctica, Southern California and North Mexico show much higher cloud-free frequencies than the global average during most seasons. In the Middle East, North Africa, South Africa, Australia, Southern California and North Mexico, the highest frequency was observed in the Boreal Summer, and the lowest in the Boreal Winter. In contrast, in Antarctica, the highest frequency was in the Boreal Winter, and the lowest in the Boreal Summer. A comparison between the cloud-free frequency images and a world desert map showed that there is good correlation between the distribution of deserts and frequent cloud free conditions, which is to be expected.

5. Discussion and conclusions

Based on the successful applications of MERIS-based and MODIS-based correction models, two advanced InSAR atmospheric correction models have been demonstrated using both MERIS and MODIS near IR water vapour products: (1) The MERIS/MODIS combination correction model (MMCC) uses MERIS data collected on date 1 and

MODIS data collected on date 2, or vice versa, to produce a ZPDDM for InSAR atmospheric correction; and (2) the MERIS/MODIS stacked correction model (MMSC) averages MERIS and MODIS data to produce a ZPDDM. Since MODIS and MERIS have different spatial resolutions from SAR data (e.g. 1000 m for MODIS, 1200 m for RR MERIS, 300 m for FR MERIS and 20~160 m for ENVISAT), both MERIS and MODIS data were resampled to a common uniform geographic grid of c. 300 m followed by low-pass filtering with an averaging window of ~2.0 km. This indicates that the effective spatial resolution of the resultant ZPDDMs is 1~2 km. On the other hand, water vapour signals at scales of c. 2 km or greater are clearly observed in MERIS and MODIS PWV fields in Figures 3, 5 and 7. *Hanssen* [2001] recognized three regimes of atmospheric delay in interferograms (Regime I: > 2km; Regime II: 0.5-2.0 km; and Regime III: 0.01-0.5 km), and suggested that the first two regimes are atmospheric whilst the third one likely reflects noise in the data. Hence, the MMCC and the MMSC models can be used for reducing water vapour effects in Regime I (i.e. at scales of >2 km) and some in Regime II (i.e. at scales of 1~2 km). The applications of both the MMCC and the MMSC models to ENVISAT ASAR data over the SCIGN region showed a significant reduction in water vapour effects on ASAR interferograms, with the RMS differences between GPS and InSAR range changes in the LOS direction decreasing from ~10 mm before correction to ~5 mm after correction. This indicates that both the MMCC and MMSC models work as efficiently as the GPS/MODIS integrated [*Li et al.*, 2005] and/or the MERIS water vapour correction models [*Li et al.*, 2006c]. Moreover, the MMSC model appeared to provide the most reliable solutions with smaller amplitudes of water vapour errors in interferograms. It is expected that these two advanced water vapour correction models will expand the application of MODIS and MERIS data for InSAR atmospheric correction.

This paper has also shown the impact of the time difference between MODIS and SAR data acquisitions on MODIS-based/related water vapour correction models for the first time. It appears that the impact depends on the temporal water vapour variation. The impact can be trivial with a time difference of around 65 minutes for some dates but can be too great to neglect, even with shorter time differences, for other dates. This suggests that an investigation into temporal water vapour variations is a pre-requisite before applying *any* correction model that contains MODIS data, which can be done by comparing MERIS with Terra MODIS data or comparing Terra with Aqua MODIS data.

This study revealed that stripes present in Terra MODIS PWV products due to radiometric calibration errors and in MERIS PWV products due to smile effects may represent another limitation for MERIS/MODIS water vapour correction models. An effective approach has been developed to destripe Terra MODIS PWV images due to the regular appearance of the stripes. However, further research is required to characterise the special behaviour of MERIS camera 4 and hence to destripe MERIS PWV images.

A simple technique for discriminating a real geophysical signal from an artefact due to stripes and/or failure to identify cloudy pixels in MERIS and/or MODIS water vapour products is to determine whether a signal is coincident with the presence of stripes and/or clouds. If this is the case, then the signal is most likely to be due to errors in water vapour products. If independent water vapour datasets (e.g. GPS, MERIS, MODIS, etc.) are available, comparisons between different water vapour correction models can also be performed to identify errors introduced by water vapour products.

Since MERIS and MODIS near-IR water vapour products are sensitive to the presence of clouds, the frequency of cloud free conditions has been investigated on a global scale

using 6 years of Terra MODIS Atmosphere Monthly Global Product for the first time. Although the global average cloud-free frequency is only ~25% [*Wylie et al.*, 1999], it has been shown that the Middle East, North Africa, South Africa, Australia, Chile, Antarctica, Southern California and North Mexico show much higher frequencies than the global average during most seasons. Note that most of the aforementioned regions are tectonically active. For example, the divergent plate boundary between the Arabian and African plates and the convergent plate boundary between the Arabian and Eurasian plates are both of great interest to a wide community of geophysicists and have frequent cloud-free conditions. This suggests that MERIS and MODIS based/related water vapour correction models show promise for correcting InSAR measurements.

Acknowledgments. This work has been carried out as part of the activities of the NERC Earth Observation Centre of Excellence: Centre for the Observation and Modelling of Earthquakes and Tectonics (COMET). Part of this research was carried out at JPL/Caltech under contract with NASA. We are grateful to A. Sibthorpe for useful discussions. We thank JPL/Caltech for the use of the ROI_PAC software to generate our interferograms [*Rosen et al.*, 2004]. Figures were prepared using the public domain Generic Mapping Tools [*Wessel and Smith*, 1998]. The ASAR and MERIS data were supplied under ESA ENVISAT data grants AOE.853 and C1P.2525 and C1P.3336, and the GPS data were obtained from the Scripps Orbit and Permanent Array Centre (SOPAC, http://sopac.ucsd.edu).

References

Abdelfattah, R., and J. M. Nicolas (2002), Topographic SAR Interferometry Formulation for High-Precision DEM Generation, *IEEE Trans. Geosci. Remote Sens.*, 40, 2415-2426.

Ackerman, S. A., K. I. Strabala, V. B. Mendes, R. A. Frey, C. C. Moeller, and L. E. Gumley (1998). Discriminating clear sky from clouds with MODIS, J. Geophys. Res., 103(D24), 32,141– 32,157.

Albert, P., R. Bennartz, and J. Fischer (2001). Remote Sensing of Atmospheric Water Vapor from Backscattered Sunlight in Cloudy Atmospheres, J. Atmos. Ocean. Tech., 18 (6), 865-874.

Argus, D.F., M.B. Heflin, G. Peltzer, F. Crampé, and F.H. Webb (2005). Interseismic strain accumulation and anthropogenic motion in metropolitan Los Angeles, J. Geophys. Res, 110 (B4), B04401, doi: 10.1029/2003JB002934.

Bawden, G.W., W. Thatcher, R.S. Stein, K.W. Hudnut, and G. Peltzer (2001). Tectonic contraction across Los Angeles after removal of groundwater pumping effects, Nature, 412 (23), 812-815.

Bennartz, R., and J. Fischer (2001). Retrieval of columnar water vapour over land from back-scattered solar radiation using the Medium Resolution Imaging Spectrometer (MERIS), Remote Sensing Environ., 78, 271-280.

Delwart, S., R. Preusker, L. Bourg, R. Santer, D. Ramon, and J. Fischer (2007), MERIS in-flight spectral calibration, International Journal of Remote Sensing, 28, 479-496.

European Space Agency (2004). MERIS Product Handbook, Issue 1.3. (Available at: http://envisat.esa.int/dataproducts/meris)

Farr, T.G., and M. Kobrick (2000). Shuttle Radar Topography Mission produces a wealth of data, Eos Trans. AGU, 81, 583-585.

Fialko, Y. (2004). Evidence of fluid-filled upper crust from observations of postseismic deformation due to the 1992 Mw7.3 Landers earthquake, J. Geophys. Res., 109, B08401, doi:10.1029/2004JB002985.

Fielding, E.J., M. Talebian, P.A. Rosen, H. Nazari, J.A. Jackson, M. Ghorashi, and M. Berberian (2005). Surface ruptures and building damage of the 2003 Bam, Iran, earthquake mapped by satellite synthetic aperture radar interferometric correlation, J. Geophys. Res., 110, B3, B03302, 10.1029/2004JB003299.

Fischer, J., and R. Bennartz, Retrieval of total water vapour content from MERIS measurements (ATBD), ESA reference number PO-TN-MEL-GS-005, ESA-ESTEC, Noordwijk, Netherlands, 1997.

Gao, B. C., and Y. J. Kaufman (2003). Water vapor retrievals using Moderate Resolution Imaging Spectroradiometer (MODIS) nearinfrared channels, J. Geophys. Res., 108(D13), 4389, doi:10.1029/2002JD003023.

HANSSEN, R., 2001, Radar Interferometry: Data interpretation and error analysis (Dordrecht: Kluwer Academic Publishers).

Hoffmann, J., and H. Zebker (2003). Prospecting for horizontal surface displacements in Antelope Valley, California using satellite radar interferometry, J. Geophys. Res., 108 (F1), 6011, doi: 10.1029/2003JF000055.

King, M.D., W.P. Menzel, Y.J. Kaufman, D. Tanre, B.C. Gao, S. Platnick, S.A. Ackerman, L.A. Remer, R. Pincus, and P.A. Hubanks (2003). Cloud and aerosol properties, precipitable water, and profiles of temperature and water vapor from MODIS, *IEEE Trans. Geosci. Remote Sens.*, 41 (2), 442-458.

Lanari, R., P. Lundgren, M. Manzo, and F. Casu (2004). Satellite radar interferometry time series analysis of surface deformation for Los Angeles, California, Geophys. Res. Lett., 31 (23), L23613, 10.1029/2004GL021294.

Li, Z. (2004). Production of regional 1 km × 1 km water vapor fields through the integration of GPS and MODIS data, paper presented at ION GNSS 2004, Inst. of Navig., Long Beach, Calif., 21–24 Sept, 2004.

Li, Z. (2005). Correction of atmospheric water vapour effects on repeat-pass SAR interferometry using GPS, MODIS and MERIS data, PhD thesis, University College London, London.

Li, Z., E. J. Fielding, and P. Cross (2006a), Separating slow deformation signals from water vapour and orbital errors using a single InSAR interferogram (Invited), *AGU Fall Meeting 2006*, San Francisco, CA, USA, 11–15 December 2006.

Li, Z., E.J. Fielding, P. Cross, and J.-P. Muller (2006b). Interferometric synthetic aperture radar atmospheric correction: GPS topography-dependent turbulence model, *J. Geophys. Res.*, 111 (B2), B02404, doi:10.1029/2005JB003711.

Li, Z., E.J. Fielding, P. Cross, and J.-P. Muller (2006c). Interferometric synthetic aperture radar atmospheric correction: MEdium Resolution Imaging Spectrometer and Advanced Synthetic Aperture Radar integration, Geophys. Res. Lett., 33, L06816, doi:10.1029/2005GL025299.

Li, Z., J.-P. Muller, and P. Cross, Comparison of precipitable water vapor derived from radiosonde, GPS, and Moderate-Resolution Imaging Spectroradiometer measurements, *J. Geophys. Res.*, 108 (D20), 4651, doi:10.1029/2003JD003372, 2003.

Li, Z., J.-P. Muller, P. Cross, P. Albert, J. Fischer, and R. Bennartz (2006d). Assessment of the potential of MERIS near-infrared water vapour products to correct ASAR interferometric measurements, Int. J. Remote Sens., 27, 349-365, doi: 10.1080/01431160500307342.

Li, Z., J.-P. Muller, P. Cross, and E.J. Fielding (2005). Interferometric synthetic aperture radar (InSAR) atmospheric correction: GPS, Moderate Resolution Imaging Spectroradiometer (MODIS), and InSAR integration, J. Geophys. Res., 110, B03410, doi:10.1029/2004JB003446.

Lin, Q., J. F. Vesecky, and H. A. Zebker (1991), Topography estimation with interferometric synthetic aperture radar using fringe detection, *Geoscience and Remote Sensing Symposium, 1991. IGARSS '91. Remote Sensing: Global Monitoring for Earth Management., International*.

Lu, Z., and W.R. Danskin (2001). InSAR analysis of natural recharge to define structure of a ground-water basin, San Bernardino, California, Geophys. Res. Lett., 28 (13), 2661-2664.

Massonnet, D., and K. L. Feigl (1998), Radar interferometry and its application to changes in the earth's surface, *Rev. Geophys.*, 36, 441-500.

Nikolaidis, R. (2002), Observation of geodetic and seismic deformation with the Global Positioning System, PhD thesis, Univ. of Calif., San Diego.

Nishihama, M., R. Wolfe, D. Solomon, F. Patt, J. Blanchette, A. Fleig, and E. Masuoka (1997). MODIS Level 1A Earth Location: Algorithm Theoretical Basis Document (Version 3.0), pp. 147, NASA/Goddard Space Flight Center, Greenbelt, MD.

Rosen, P. A., S. Hensley, I. R. Joughin, F. K. Li, S. N. Madsen, E. Rodriguez, and R. M. Goldstein (2000), Synthetic aperture radar interferometry - Invited paper, *Proc. IEEE*, 88, 333-382.

Rosen, P.A., S. Hensley, G. Peltzer, and M. Simons (2004). Updated Repeat Orbit Interferometry package released, Eos Trans. AGU, 85 (5), 47.

Scharroo, R., and P. Visser (1998). Precise orbit determination and gravity field improvement for the ERS satellites, J. Geophys. Res., 103 (C4), 8113-8127.

Watson, K.M., Y. Bock, and D.T. Sandwell (2002). Satellite interferometric observations of displacements associated with seasonal groundwater in the Los Angeles basin, J. Geophys. Res., 107 (B4), 2074, 10.1029/2001JB000470.

Wessel, P., and W.H.F. Smith (1998). New, improved version of the Generic Mapping Tools released, EOS Trans. AGU, 79, 579.

Wright, T.J., B. Parsons, P.C. England, and E.J. Fielding (2004). InSAR observations of low slip rates on the major faults of western Tibet, Science, 305 (5681), 236-239.

Wylie, D.P., and W.P. Menzel (1999). Eight Years of High Cloud Statistics Using HIRS, J. Climate, 12 (1), 170-184.

Zebker, H. A., and R. M. Goldstein (1986), Topographic Mapping from Interferometric Synthetic Aperture Radar Observations, *J. Geophys. Res.*, 91, 4993-4999.

Zebker, H.A., P.A. Rosen, and S. Hensley (1997). Atmospheric effects in interferometric synthetic aperture radar surface deformation and topographic maps, J. Geophys. Res., 102 (B4), 7547-7563.

Table 1. Details of interferograms (Ifms) used in this study

	Track	Date 1	Time Diff 1 [a] (min)	Date 2	Time Diff 2 [a] (min)	δt (days)	$B_{\perp}$(m) [b]	σ (radians) [c]
Ifm1	170	27-Sep-2003	+65	29-Jan-2005	+5	490	-217 to -247	1.21
Ifm2	170	07-Aug-2004	+50	09-Apr-2005	+65	245	-30 to -92	0.45
Ifm3	170	14-May-2005	+0	27-Aug-2005	+5	105	-117 to -83	0.57

[a] Time difference between ASAR and Terra MODIS acquisitions. Positive implies that MODIS over-pass time was later than ASAR.
[b] Perpendicular baseline at center of swath which varies along the track between the values shown.
[c] Maximum phase error due to the topographic uncertainty of SRTM DEM (7 m, *Farr and Kobrick* [2000]).

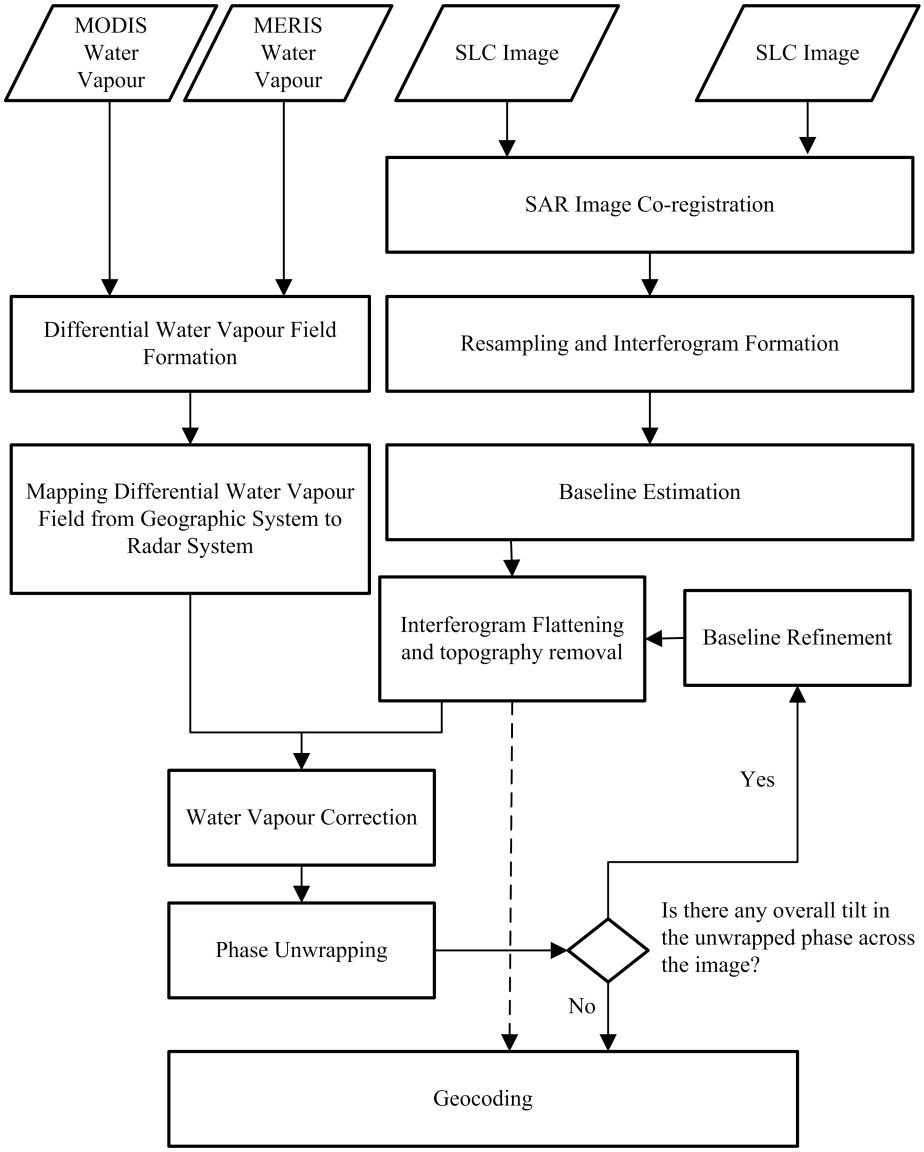

Figure 1. Flowchart of InSAR processing with MERIS/MODIS combination correction model (MMCC).

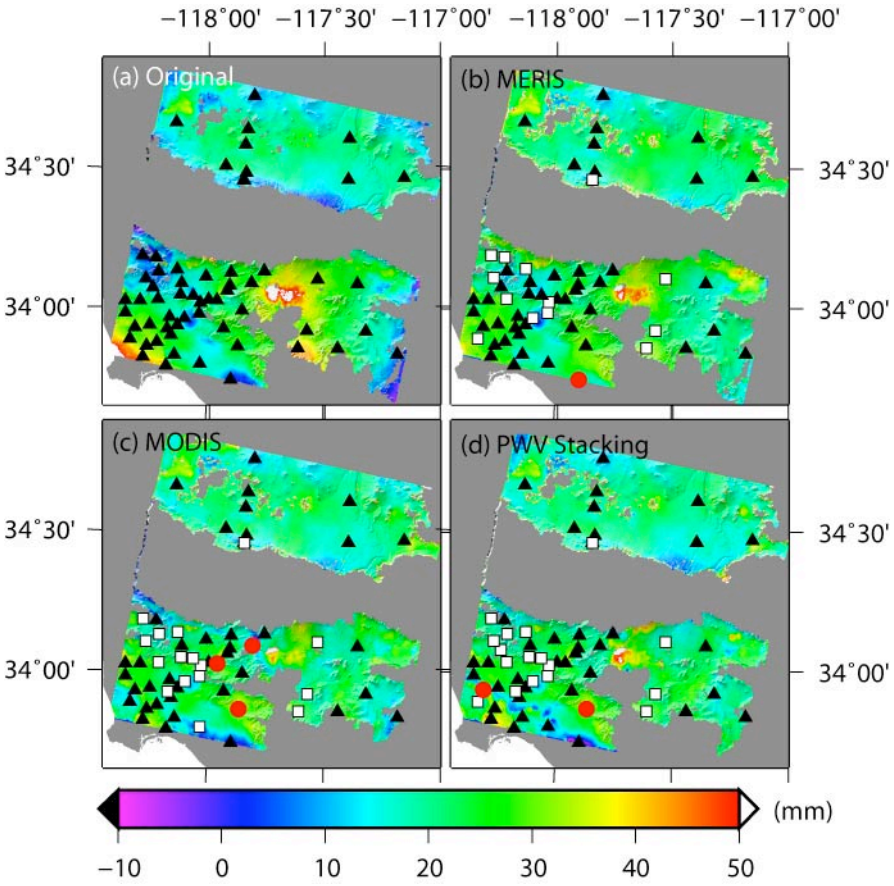

Figure 2. Ifm1 superimposed on a SRTM DEM. (a) Original Ifm: 030927-050129; (b) Corrected Ifm using MERIS water vapour correction model; (c) Corrected Ifm using MODIS water vapour correction model; (d) Corrected Ifm using MERIS/MODIS stacking correction model (i.e. MERIS + MODIS (date 1) – MERIS + MODIS (date 2)). Note: (1) Positive implies that the surface moves away from the satellite, i.e. the pixel exhibits subsidence, and negative implies uplift in LOS; (2) The black solid triangles represent GPS stations where the differences between InSAR-derived and GPS-derived range changes are within a 1-sigma range both before and after correction; (3) White squares with black borders imply improvement after correction; (4) Red solid circles indicate deterioration after correction.

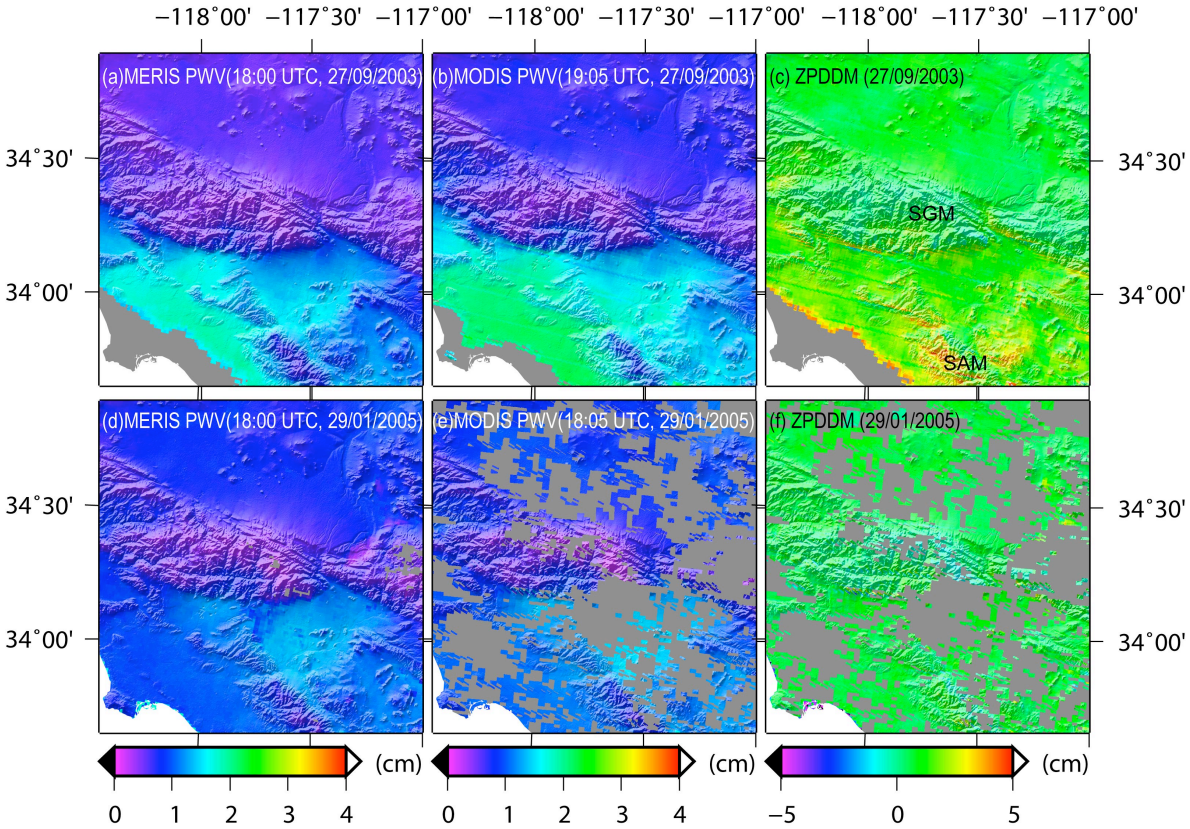

Figure 3. Water vapour fields or ZPDDMs superimposed on a SRTM DEM. (a) MERIS PWV collected at 18:00 UTC on 27 September 2003; (b) MODIS PWV collected at 19:05 UTC on 27 September 2003; (c) ZPDDM = (MODIS^{b} – MERIS^{a}) × 6.2; SGM stands for San Gabriel Mountains, and SAM for Santa Ana Mountains; (d) MERIS PWV collected at 18:00 UTC on 29 January 2005; (e) MODIS PWV collected at 18:05 UTC on 29 January 2005; (f) ZPDDM = (MODIS^{e} – MERIS^{d}) × 6.2. Note: Grey represents cloudy pixels.

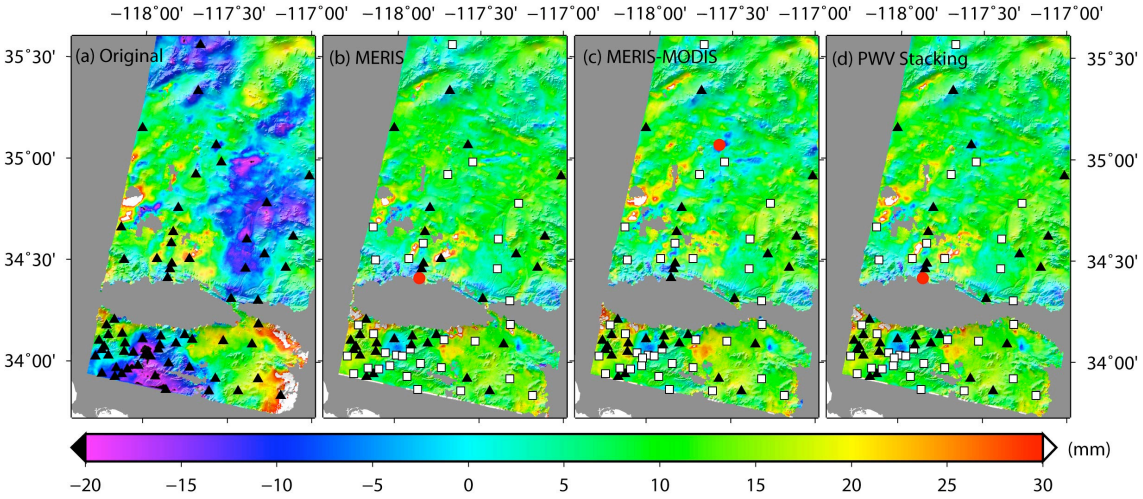

Figure 4. Ifm2 superimposed on a SRTM DEM. (a) Original Ifm: 040807-050409; (b) Corrected Ifm using MERIS correction model; (c) Corrected Ifm using the MMCC model (i.e. MERIS (date 1) – MODIS (date 2)); (d) Corrected Ifm using the MMSC model (i.e. MERIS (date 1) – MERIS + MODIS (date 2)).

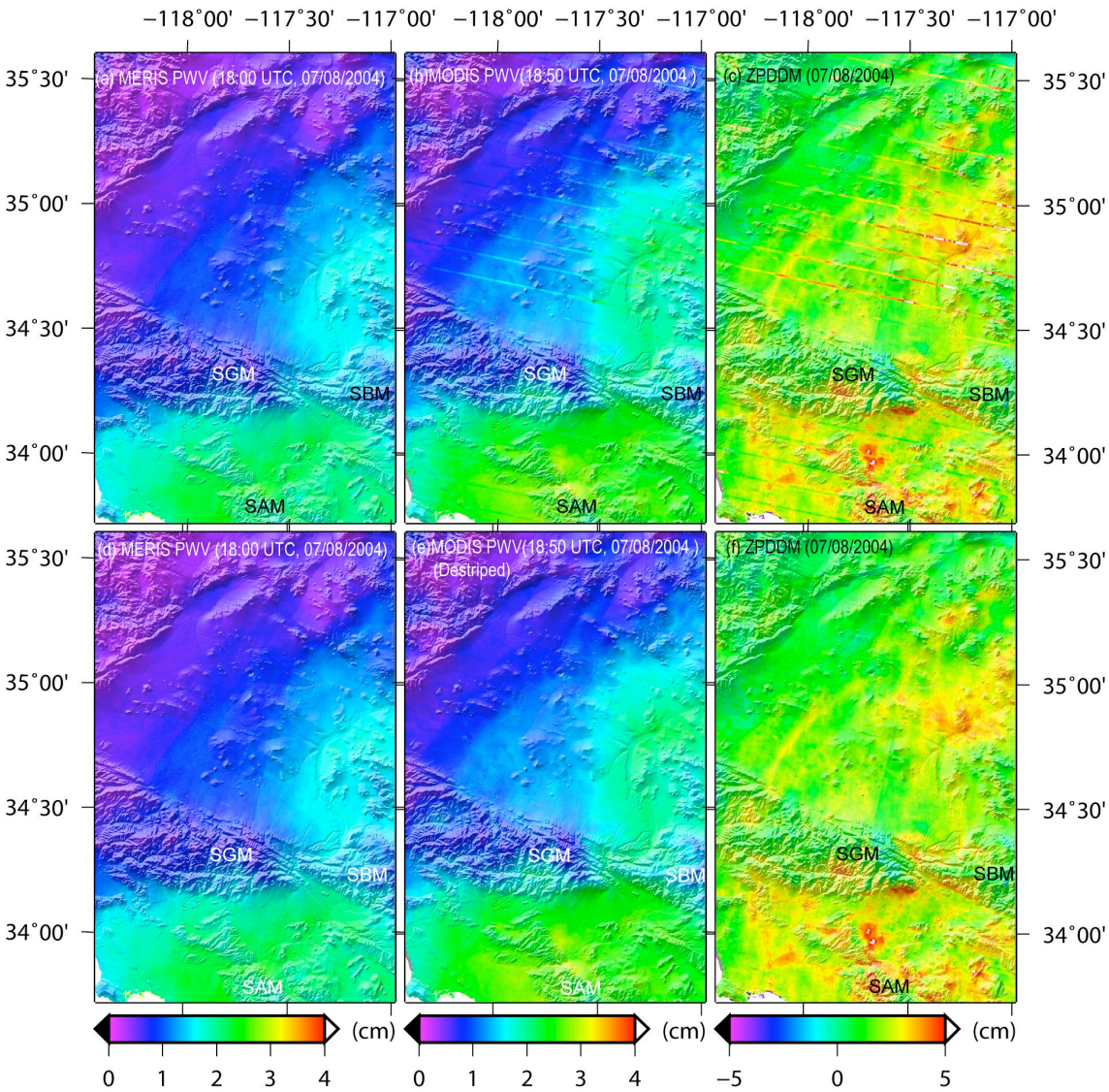

Figure 5. Water vapour fields or ZPDDMs superimposed on a SRTM DEM. (a) MERIS PWV collected at 18:00 UTC on 7 August 2004; (b) MODIS PWV collected at 18:50 UTC on 7 August 2004; (c) ZPDDM = (MODIS^{b} – MERIS^{a}) × 6.2; (d) MERIS PWV same as (a); (e) MODIS PWV same as (b) but destriped; (f) ZPDDM = (MODIS^{e} – MERIS^{d}) × 6.2. Note: Grey represents cloudy pixels; SGM stands for San Gabriel Mountains, SBM for San Bernardino Mountains and SAM for Santa Ana Mountains;

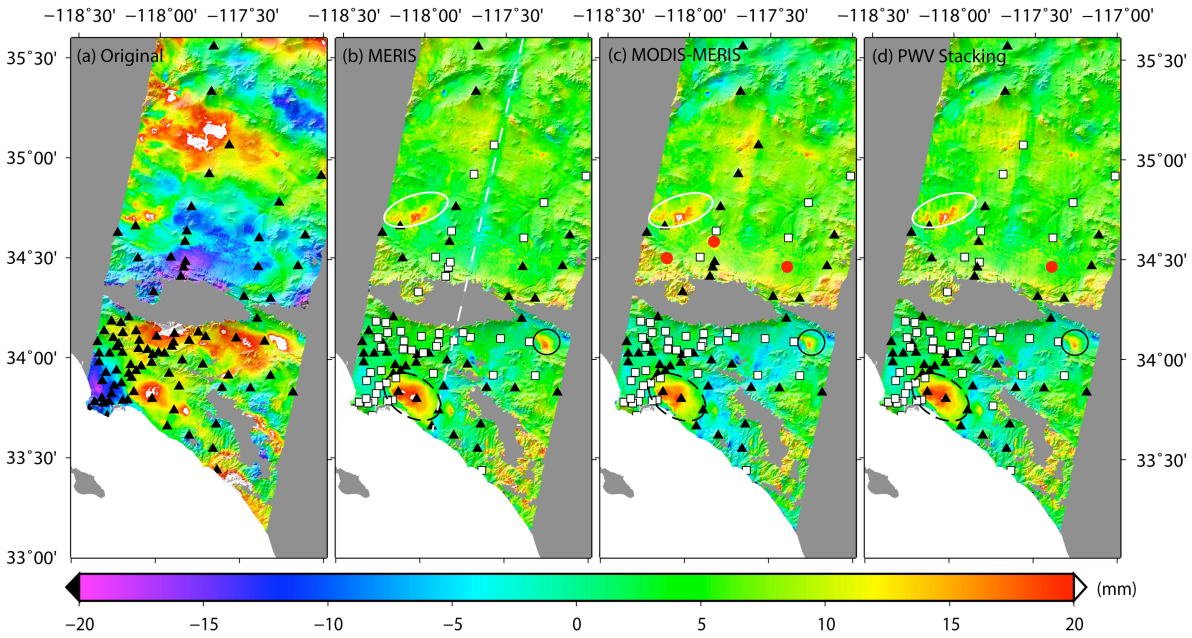

Figure 6. Ifm3 superimposed on a SRTM DEM. (a) Original Ifm: 050514-050827; (b) Corrected Ifm using MERIS correction model; (c) Corrected Ifm using the MMCC model (i.e. MODIS (date 1) – MERIS (date 2)) ; (d) Corrected Ifm using the MMSC model (i.e. MERIS + MODIS (date 1) – MERIS (date 2)). Note: (1) The black dashed oval indicates surface subsidence in the Long Beach-Santa Ana basin; (2) The white solid oval implies surface subsidence in Antelope Valley; (3) The black solid circle represents geophysical signals in San Bernardino; (4) The white dashed line represents a camera border on the MERIS water vapour field collected on 27 August 2005.

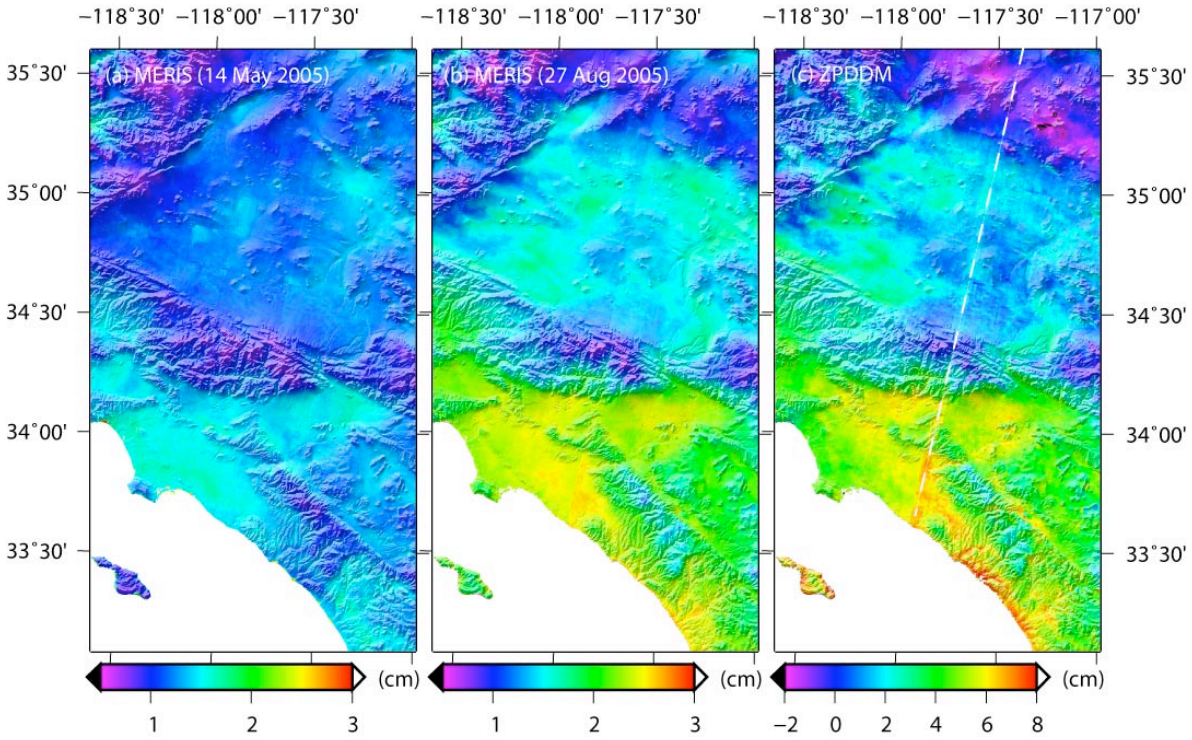

Figure 7. Water vapour fields or ZPDDM superimposed on a SRTM DEM. (a) MERIS PWV collected on 14 May 2005; (b) MERIS PWV collected on 27 August 2005; (c) ZPDDM = ($MERIS^{b}$ – $MERIS^{a}$) × 6.2. Note: The white dashed line represents a camera border on the MERIS water vapour field collected on 27 August 2005.

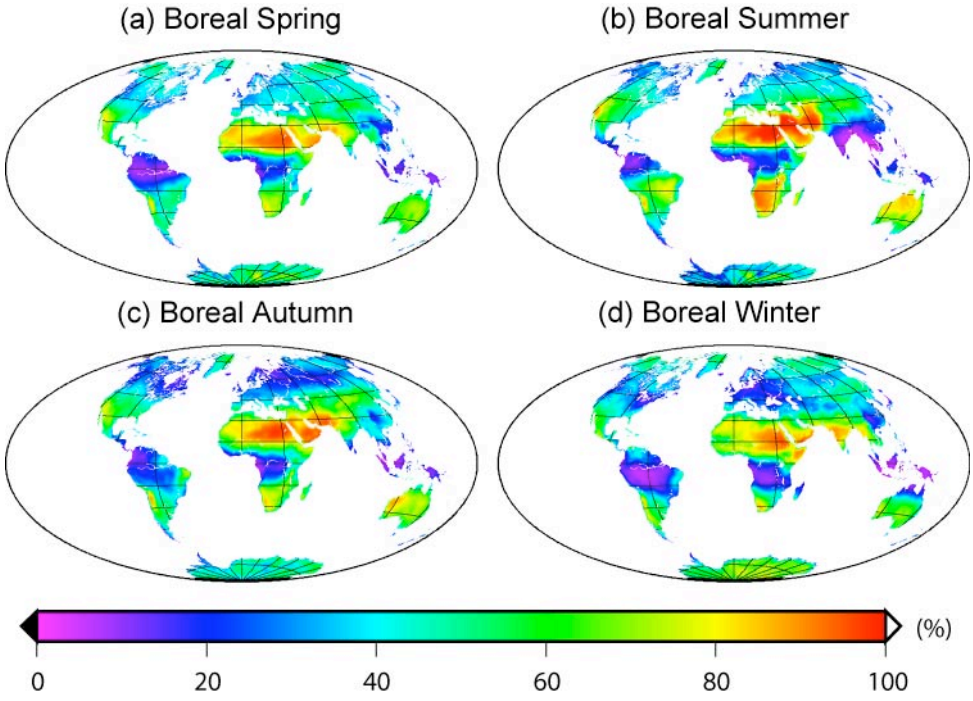

Figure 8. Seasonal frequencies of cloud free conditions across the globe during the period from March 2000 to February 2006. (a) Boreal Spring (March-May). (b) Boreal Summer (June–August). (c) Boreal Autumn (September–November). (d) Boreal Winter (December–February).